

Underwater Image Enhancement via Weighted Wavelet Visual Perception Fusion

Weidong Zhang[✉], Member, IEEE, Ling Zhou, Peixian Zhuang[✉], Guohou Li, Xipeng Pan[✉], Wenyi Zhao[✉], and Chongyi Li[✉], Senior Member, IEEE

Abstract—Underwater images typically suffer from various quality degradation issues due to the scattering and absorption of light, but these degraded-quality underwater images are unbenevolent for analysis and applications. To effectively solve these quality degradation issues, an underwater image enhancement method via weighted wavelet visual perception fusion is introduced, called WWPF. Concretely, we first present an attenuation-map-guided color correction strategy to correct the color distortion of an underwater image. Subsequently, we employ the maximum information entropy optimized global contrast strategy to the color-corrected image to obtain a global contrast-enhanced image. Meanwhile, we apply a fast integration optimized local contrast strategy to the color-corrected image to get a local contrast-enhanced image. To exploit the complementary of the global contrast-enhanced image and the local contrast-enhanced image, we introduce a weighted wavelet visual perception fusion strategy to obtain a high-quality underwater image by fusing the high-frequency and low-frequency components of images at different scales. Our extensive experiments on three benchmarks validate that our WWPF outperforms the state-of-the-art methods in qualitative and quantitative. Besides, the underwater images processed by our WWPF also benefit practical underwater applications. The code is available https://github.com/Li-Chongyi/WWPF_code.

Index Terms—Underwater image enhancement, color correction, light scattering, contrast enhancement, underwater imaging.

Manuscript received 26 April 2023; revised 28 June 2023; accepted 24 July 2023. Date of publication 27 July 2023; date of current version 5 April 2024. This work was supported in part by the Natural Science Foundation of Henan Province under Grant 232300420428, in part by the National Natural Science Foundation of China under Grant 62171252, and in part by the China Post-Doctoral Science Foundation under Grant 2019M660438. This article was recommended by Associate Editor B. Zatt. (*Corresponding authors:* Peixian Zhuang; Chongyi Li.)

Weidong Zhang, Ling Zhou, and Guohou Li are with the School of Information Engineering, and the Institute of Computer Applications, Henan Institute of Science and Technology, Xinxiang 453003, China (e-mail: zwd_wd@163.com; zhoul20211116@163.com; liguohou6@163.com).

Peixian Zhuang is with the School of Automation and Electrical Engineering, University of Science and Technology Beijing, Beijing 100083, China (e-mail: zhuangpeixian0624@163.com).

Xipeng Pan is with the School of Computer Science and Information Security, Guilin University of Electronic Technology, Guilin 541004, China (e-mail: pxp201@guet.edu.cn).

Wenyi Zhao is with the School of Artificial Intelligence, Beijing University of Posts and Telecommunications, Beijing 100876, China (e-mail: 2013211876@bupt.edu.cn).

Chongyi Li is with the School of Computer Science, Nankai University, Tianjin 300071, China (e-mail: lichongyi@nankai.edu.cn).

This article has supplementary material provided by the authors and color versions of one or more figures available at <https://doi.org/10.1109/TCSVT.2023.3299314>.

Digital Object Identifier 10.1109/TCSVT.2023.3299314

I. INTRODUCTION

THE ocean is closely related to the production and life of humans, covering 71% of the Earth's surface. Meanwhile, it is an essential part of the Earth's living system. In developing and utilizing marine resources, underwater images are an important carrier and presentation form to understand and perceive the underwater world [1]. However, underwater images are seriously degraded by the complicated physical environment underwater [2]. On the one hand, light absorption easily leads to color cast, low contrast, and brightness reduction in underwater images [3]. On the other hand, light scattering easily leads to problems such as fog blur, detail loss, and noise amplification of underwater images [4]. Low-quality underwater images seriously affect the visual perception of human eyes, and it also challenges the subsequent analysis and processing of images. Thus, research on effective underwater image sharpness methods has become a crucial problem to be solved urgently in underwater vision.

Currently, the existing underwater image enhancement methods [5], [6] can be grouped into three categories, which include image restoration, image enhancement, and deep learning methods, respectively. In the early stages, image restoration-based methods relied on some priors to recover clear underwater images. However, too many priors challenge the effectiveness and robustness of such methods [7]. Unlike image restoration methods, image enhancement-based methods without consider priors to improve the contrast and brightness of the underwater images by correcting pixel values. Unfortunately, they tend to introduce the appearance of over-enhancement or over-saturation in the enhanced images [8], [9]. Recently, deep learning methods [10], [11], [12], [13] have been gradually applied to underwater image enhancement thanks to the massive amount of training data. Noteworthy, the high-quality, large-scale, and paired underwater images are uneasily accessible, thus limiting the performance of deep learning methods. Meanwhile, the complex and changeable underwater environment easily cause the unstable performance of deep learning methods. To sum up, it is worthwhile to investigate how to integrate the advantages of different methods to improve the quality of underwater images and the performance of underwater image enhancement methods.

In our work, we proposed a **Weighted Wavelet visual Perception Fusion** method to enhance underwater images, called **WWPF**. Unlike earlier fusion strategies [9], [16], our

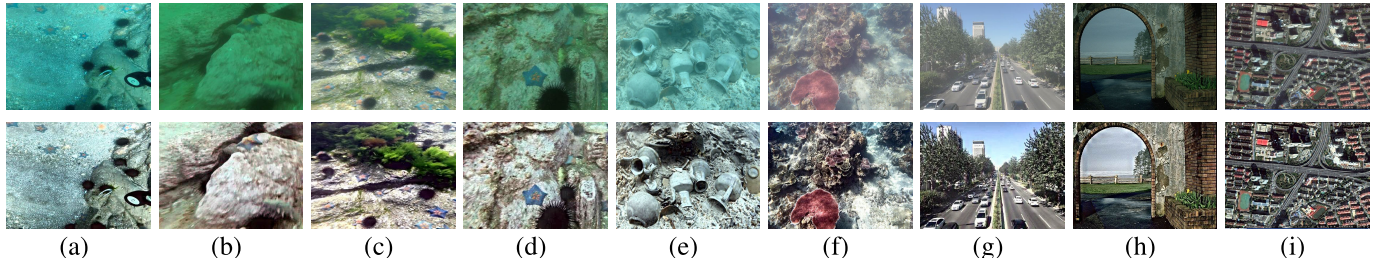


Fig. 1. Enhanced results (bottom) of our WWPF for several raw images (top). (a) and (b) are derived from the UCCS [14]. (c) and (d) are derived from the UIQS [14]. (e) and (f) are derived from the UIEB [15]. (g), (h), and (i) are derived from the Internet. Without fine-tuning the parameters, our WWPF obtained satisfactory visual results for different degraded images from different datasets.

WWPE utilizes different scales of high- and low-frequency components instead of different scales of weight maps in fusion methods to integrate the complementary advantages of different enhanced versions of images. Our WWPF focuses on exploring how to effectively improve the color, global contrast, and local contrast of underwater images, and it consists of three key stages: attenuation-map-guided color correction, global and local contrast enhancement, and weighted wavelet visual perception fusion. In the first stage, we redefine the different color channels and employ the luminance channel as the reference channel to obtain a color transfer image by compensating the other three color channels. Meanwhile, we utilize an attenuation map to guide the fusion of the input and color transfer images to obtain a color-corrected image. Subsequently, we adopt the maximum information entropy optimized global contrast strategy and the fast integration optimized local contrast strategy to apply on the color-corrected image to obtain a global contrast-enhanced image and a local contrast-enhanced image. At last, we employ a wavelet decomposition strategy for the global and local contrast-enhanced images to get high- and low-frequency components with different scales. Meanwhile, we utilize the weighted wavelet perception fusion strategy to reconstruct a high-quality underwater image by integrating different levels of components with different scales. Additionally, Fig. 1 presents the enhanced results of our WWPF for several degraded images.

- We introduce an attenuation-map-guided color correction strategy for correcting the color cast of underwater images, which considers not only the grey-scale assumption that each color channel retains similar average grey values before attenuation, but also the fact that different light attenuation leads to various color distortions in underwater images.
- We propose a maximum information entropy-optimized global contrast strategy and a fast integration-optimized local contrast strategy to improve the global and local contrast of the color-corrected image, respectively. We found that the advantageous complementary features of the global and local contrast-enhanced images can effectively improve the quality of underwater images.
- We present a weighted wavelet visual perception fusion strategy, which uses the wavelet decomposition method to get the approximate low-frequency component and the vertical, horizontal, and diagonal high-frequency components of the global and local contrast-enhanced

images. Afterward, we employ the weighted inverse wavelet transform strategy to reconstruct a high-quality underwater image by exploiting the advantages of different level components with different scales.

The rest of the paper is organized and detailed below. Section II details the related research work in underwater image enhancement. Section III describes the workflow for each step of our WWPF method. Section IV gives a detailed overview of the experimental results and analysis. In the last section, we summarize and look forward to our work.

II. RELATED WORK

Currently, underwater image enhancement techniques are grouped into three main categories: image restoration, image enhancement, and deep learning methods [17], [18], [19]. A brief overview of the current research is as follows.

Image restoration methods use some priors to estimate the underwater imaging parameters and invert the degradation process to obtain clear underwater images [20], [21]. Recently, the dark channel prior (DCP) has been successfully applied to underwater image restoration thanks to the similar degradation characteristics of the underwater and foggy images [22], [23], [24]. These priors mainly contain general dark channel prior [25], attenuation curve prior [26], submerged dark channel prior [27], statistical prior [28], haze lines prior [29], etc. Wang et al. [26] statistical the pixel distribution of clear images in RGB space proposed an adaptive fading curve prior for estimating more accurate transmission maps, but the complex optimization process led to the sensitive robustness of the model. Berman et al. [29] considered multiple spectral profiles of different water types and estimated two additional global parameters to defog underwater images, which could correct color distortion and restore the 3D structure of underwater scenes, but it had relatively high time complexity. Muniraj et al. [30] estimated the depth of the transmission map by using the difference in the intensity of each channel, which was complicated in processing steps. Liang et al. [31] proposed a generalized imaging model for the restoration of low-quality images, which combined multiple prior such as the grey-scale world to construct an image decomposition objective function. However, these methods rely on some priors, in which the performance of single-prior hypothesis methods needs to be improved. In contrast, multiple prior methods face difficulties in optimizing various parameters.

Image enhancement methods improve the color, contrast, and sharpness of underwater images by adjusting the

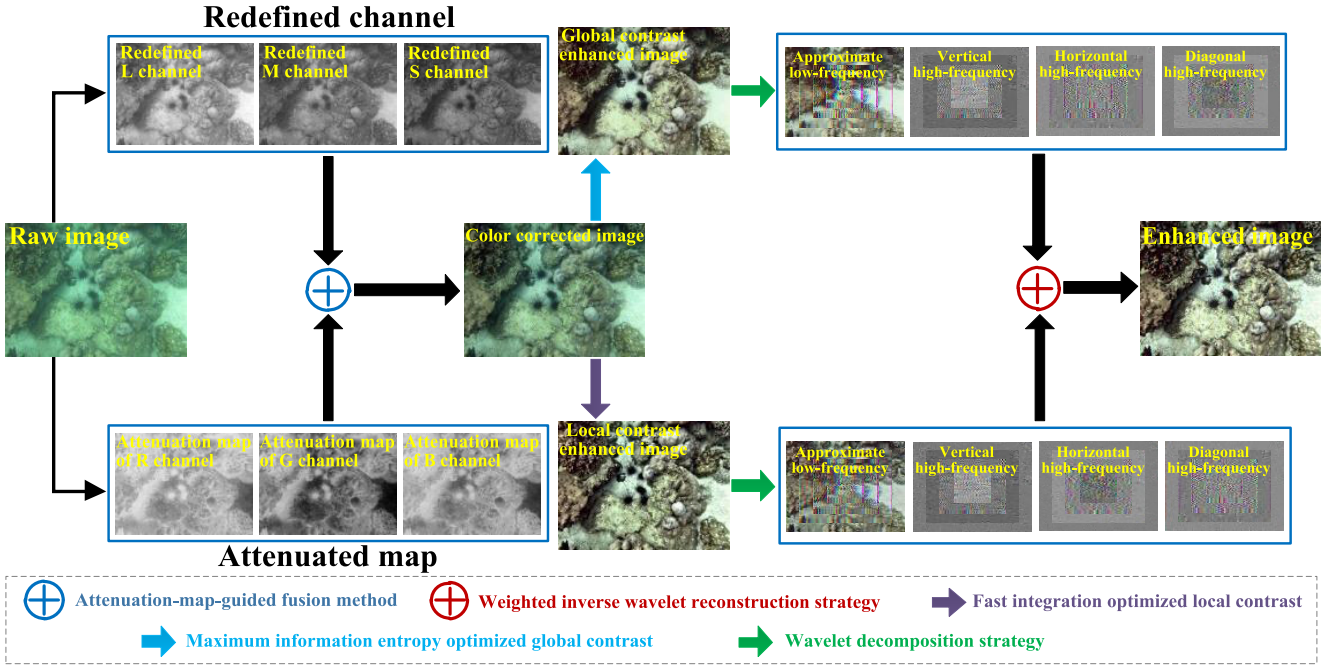


Fig. 2. Flowchart of our proposed WWPF method. Given a raw underwater image, it first participates in an attenuation-map-guided color correction stage to produce a color-corrected underwater image. Afterward, two images are denoted as the global contrast-enhanced and the local contrast-enhanced images. They are derived from the color-corrected image obtained by the maximum information entropy optimized global contrast method and the fast integration optimized local contrast method. Finally, the two enhanced versions of the approximate low-frequency component, vertical, horizontal, and diagonal high-frequency components, are used to reconstruct a high-quality underwater image.

pixel value of the image, which is represented by the Retinex [32], [33], [34], histogram [35], [36], [37], and fusion methods [16], [38], [39], [40], [41]. For example, Zhang et al. [9] proposed a Retinex-inspired color correction and detail-preserved fusion method to enhance underwater images, which had an over-enhancement problem in the enhanced images. Zhuang et al. [32] proposed a variational Retinex method based on the advantages of $L_{1/2}$ norm and L_2 norm, which better enhanced the contrast and texture details of underwater images, but introduced micro-red distortion. Chani et al. [35] proposed a recursive adaptive histogram modification method to remit the issues of under-enhancement and over-enhancement in the early use of histograms. Ancuti et al. [16] proposed a color balance and fusion method that integrates the advantages of the contrast-enhanced image and the detail-sharpened image from a white-balanced image. Jiang et al. [39] introduced a local structural batch decomposition strategy based on the previous fusion [16], which ignores non-uniform illumination to the extent that it does not effectively address the halo effect. Overall, they only consider basic information about the image itself, which means they cannot effectively address color distortion and halo effects in underwater images.

Deep learning methods aim to automatically extract representation features from training data and establish a nonlinear mapping relationship, which is represented by CNN (Convolutional Neural Network) and GAN (Generative Adversarial Network) [42], [43], [44]. Depending on the powerful computing devices and abundant training data, deep learning methods are gradually applied to low-level visual tasks [45], [46], [47], [48]. Inspired by CNN [49], [50], Li et al. [15] constructed an underwater enhanced dataset containing pairs of high-quality

and low-quality underwater images to alleviate the data deficit and proposed a WaterNet for validating the enhanced performance of the dataset. Li et al. [51] proposed an underwater enhancement CNN inspired by underwater scenes prior, which utilized the water types and the degradation levels to construct synthesized underwater images. Recently, Zhao et al. [52] designed a low-weight cascade network for underwater image enhancement based on the previous CNN [51], which gives consideration to both performance and complexity. Inspired by GAN [53], [54], [55], Skinner et al. [56] constructed synthesized underwater images by the underwater physical model for GAN training, but the synthesized images are unable accurately represent the natural underwater scenes. Qi et al. [57] employed corrected feature matching and connection learning to enhance underwater images cooperatively. Liu et al. [58] designed a goal-guided twin GAN that included an edge-holding closed-loop adversarial enhancement module and a task-aware feedback module, but the excessive number of learning strategies increased the complexity of the model. In general, the type of method improves the quality of underwater images to a certain extent, but its training phase requires a large number of high-quality underwater images.

III. METHODOLOGY

We present the weighted wavelet visual perception fusion flowchart in Fig. 2. Our framework is built on a wavelet fusion, in which the two inputs are obtained by enhancing the global and local contrast of a color-corrected version from a raw underwater image. Our method mainly includes three main steps: color correction, global and local contrast enhancement, and weighted wavelet fusion. Firstly, an attenuation map-guided fusion to remove the color distortion of underwater

images caused by wavelength-dependent color absorption in the water medium. Subsequently, the global and local contrast-enhanced versions of the color-corrected image establish a complementary advantage relationship. Finally, these two enhanced versions are integrated with different levels of complementary information by weighted wavelets to produce a high-quality underwater image. Therefore, the following sections will discuss techniques for enhancing contrast and detail in underwater images.

A. Motivation

Unlike land images, underwater images typically suffer from severe and various color distortions (such as blue, green, yellow, blue-green, etc.) due to exceptional imaging and lighting limitations. Unfortunately, these color cast issues seriously affect the subjective vision of underwater images and subsequent further applications. As a result, color correction is essential in the pre-processing stage of underwater image enhancement. Nonetheless, more than color correction alone is needed to improve contrast and texture detail in underwater images. To this end, the following sections will focus on techniques to enhance the contrast and detail of the underwater image.

1) Motivation of Color Correction: Recently, statistical-based color correction [32] and piecewise color correction [59] have demonstrated their effectiveness for color correction of underwater images. However, these methods introduce some reddish casts due to excessive correction. Meanwhile, color channel compensation strategies [16], [38], [60] also positively affect the color correction of underwater images. To cope with the issues, color transfer strategies [37], [61] have been successfully applied in the color correction of underwater images thanks to the advantage of color transfer. Therefore, the color transfer method in our work is utilized to fully exploit the benefits of the piecewise color correction and color channel compensation methods.

2) Motivation of Contrast Enhancement: Histogram equalization methods [19], [62] enhance the contrast and brightness of underwater images by readjusting the histogram distribution but suffer from over-enhancement issues. Bi-histogram equalization methods [17], [36] mitigates these problems, although the Bi-histogram effectively enhances the global contrast of the images but amplifies the noise. Noteworthy, the full use of local blocks [9], [37] has provided significant advantages regarding local contrast enhancement of underwater images. Recently, fusion-based methods [35], [37] have taken advantage of the different feature maps to effectively integrate different enhanced versions to obtain a high-quality underwater image. Unlike these fusion methods, we employ a weighted wavelet fusion strategy to obtain a high-quality underwater image by integrating the high and low-frequency components of the different enhanced versions.

B. Attenuation Map Guided Color Correction

Inspired by the grayscale world hypothesis [16], each channel of the image has similar grayscale mean and histogram

distribution before attenuation. However, the individual channels of an underwater image are attenuated to varying degrees, so the traditional grey-scale world suffers from color over-correction. We redefine the channel with the maximum pixel intensity as the luminance channel, which is also known as the reference channel. Mathematically, the calculation process of the luminance channel is defined as:

$$I_l(i, j) = \max\{I_r(i, j), I_g(i, j), I_b(i, j)\}, \quad (1)$$

where I_l , I_r , I_g , and I_b are the luminance, red, yellow, and blue color channels, respectively. Subsequently, we choose the luminance channel as the reference channel to effectively compensate for the attenuation of the red, green, and blue color channels due to the absorption of light in the water medium. Specifically, the average pixel intensity of each color channel is expressed as:

$$\bar{I}_c = \frac{1}{H \times W} \sum_{i=1}^H \sum_{j=1}^W I_c(i, j), \quad c \in \{l, r, g, b\}, \quad (2)$$

where W and H are the height and width of each input channel, respectively. \bar{I}_l , \bar{I}_r , \bar{I}_g , and \bar{I}_b are the mean values of the luminance, red, green, and blue channels. Subsequently, the mean value of the luminance channel is used as a reference value to compensate for red, green, and blue channels, which is expressed as:

$$\begin{cases} I_r^C(i, j) = I_r(i, j) + (\bar{I}_l - \bar{I}_r) \times I_l(i, j) \\ I_g^C(i, j) = I_g(i, j) + (\bar{I}_l - \bar{I}_g) \times I_l(i, j) \\ I_b^C(i, j) = I_b(i, j) + (\bar{I}_l - \bar{I}_b) \times I_l(i, j), \end{cases} \quad (3)$$

where I_r^C , I_g^C , and I_b^C are the compensated red, green, and blue color channels. Although the above compensation strategy allows the underwater image to satisfy the grey-scale world assumption that each channel has approximately equal mean grey values, it does dissatisfy the histogram distribution that each channel has a similar histogram distribution. To further extend the dynamic range of each channel so that it satisfies the grey-scale world assumption that each channel has a similar histogram distribution. We further employ a linear stretching method to correct the color-compensated underwater image, which is also the color transfer image. The linear stretching process is defined as:

$$I_c^{CR} = I_o^{\min} + (I_c^C - I_c^{\min}) \times \frac{I_o^{\max} - I_o^{\min}}{I_c^{\max} - I_c^{\min}}, \quad c \in \{r, g, b\}, \quad (4)$$

where I_c^{CR} is the channel of the correction color corresponding to the c^{th} color channel. I_c^{\max} and I_c^{\min} are the maximum and minimum pixel values corresponding to the c^{th} input channel, respectively. I_o^{\max} and I_o^{\min} are the maximum and minimum stretching ranges corresponding to each color channel, they are set to 0 to 255. The grey-scale world assumption only takes into account the mean grey values and histogram distribution of the individual color channels, and it is insufficient to consider the wavelength-dependent light absorption effect of the underwater image.

Fig. 3 shows the results obtained using only the color compensation strategy for blue, green, and yellow underwater

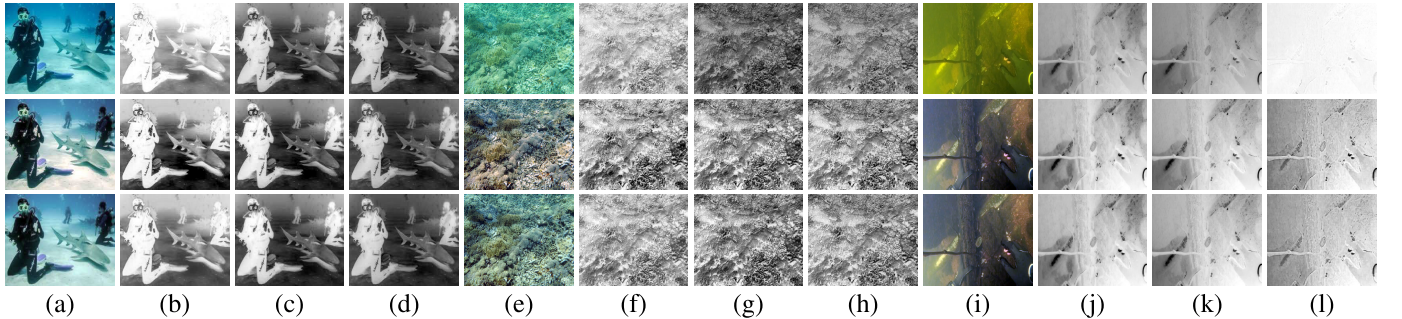


Fig. 3. Comparison results were yielded using the color compensation and attenuation-map-guided fusion. From top to bottom: (a), (e), and (i) are the raw underwater images (From left to right are blue, green, and yellow underwater images.), the result of color compensation, and the result of attenuation map-guided fusion respectively. (b), (f), and (j) are the attenuation map of the red channel, respectively. (c), (g), and (k) are the attenuation map of the green channel, respectively. (d), (h), and (l) are the attenuation map of the blue channel, respectively.

images face over-correction, slightly red, and slightly blue casts. Therefore, we thoroughly exploit the attenuation of different lights and utilize the attenuation map to guide the fusion of the raw underwater image and the color transfer image to obtain a color-corrected underwater image. To ensure that the light attenuation of each color channel can be compensated well, we utilize the maximum attenuation map as the guide fusion image. Mathematically, the maximum attenuation map is defined as:

$$I_{\max}^A = \max\{1 - I_r^\gamma, 1 - I_g^\gamma, 1 - I_b^\gamma\}, \quad (5)$$

where I_{\max}^A is the maximum attenuation map, γ is the parameter that controls the intensity of the received light, and γ as the default value of 1.2 was determined by Ancuti et al. [63]. Whereafter, we employ the attenuation map to fusion the raw underwater image and the color transfer underwater image pixel by pixel to obtain a color-corrected underwater image as:

$$I_c^{\text{CC}} = I_{\max}^A I_c^{\text{CR}} + (1 - I_{\max}^A) I_c, \quad c \in \{r, g, b\}, \quad (6)$$

where I_c^{CC} and I_c^{CR} are the color corrected and color transfer underwater images. It can be observed from Fig. 3 that although the proposed color correction method has achieved satisfactory color correction and three channels with similar attenuation, it also faces the problem of insufficient contrast and detail enhancement.

C. Optimized Global Contrast

In this section, we aim to improve the global contrast of the color-corrected image using the maximum information entropy optimized global contrast strategy. Image entropy can measure the uniform distribution of image histograms and predict the richness of image details [64]. Mathematically, entropy is defined in information theory as:

$$I_{\text{Entropy}} = - \sum_{i=0}^{L-1} p_i \log_2 p_i, \quad (7)$$

where p_i is the probability of grayscale i , L is the number of grey levels in the input image, and the dynamic range of the image is from 0 to $L - 1$. Histogram equalization leads to the integration of the histogram data of the image, which may reduce the entropy of the image. The consolidation of image grey levels may result in a loss of image detail, so the

consolidation of grey levels in the histogram can be measured against the amount of information entropy, thus ensuring that the global contrast of the image is effectively enhanced. Finally, we utilize the maximum information entropy as a metric for optimizing the global contrast in the Bi-histogram.

In optimizing global contrast, we first define the histogram data separation threshold I_{ht} and dynamic range separation threshold I_{dt} . Currently, most Bi-histogram methods directly set the two thresholds equal, but it limits the application of the Bi-histogram method. Therefore, we propose a maximum entropy optimized global contrast enhancement strategy, which has difficulty searching for the best dynamic separation threshold. Specifically, the dynamic threshold I_{dt} is traversed over the entire grey scale range. In each traversal, the method performs a stretching operation on the histograms to the left and right of the threshold. Next, the method calculates and sums the information entropy of the left and right histograms. Until the maximum value of the sum of the left and right information entropies is solved, the corresponding separation threshold point is the optimal dynamic separation threshold I_{best} . Mathematically, the maximum entropy corresponding to the optimal separation threshold is expressed as:

$$\begin{aligned} I_{\text{best}} &= \text{argmax}(I_{\text{Entropy}}(I_{ht})), \quad I_{ht} \in [0, L - 1], \\ \text{s. t. } I_{\text{Entropy}}(I_{ht}) &= I_{\text{Entropy}}^{\text{Left}}(I_{ht}) + I_{\text{Entropy}}^{\text{Right}}(I_{ht}), \end{aligned} \quad (8)$$

where $I_{\text{Entropy}}^{\text{Left}}(I_{ht})$ and $I_{\text{Entropy}}^{\text{Right}}(I_{ht})$ represent the information entropy of the left and right histograms of the optimized global contrast image, respectively. Their calculation process is expressed as:

$$\begin{aligned} I_{\text{Entropy}}^{\text{Left}}(I_{ht}) &= - \sum_{i=0}^{I_{ht}} p_i \log_2 p_i, \\ I_{\text{Entropy}}^{\text{Right}}(I_{ht}) &= - \sum_{i=I_{ht}+1}^{L-1} p_i \log_2 p_i, \end{aligned} \quad (9)$$

where P_i denotes the probability of each grey level after the sub-histogram has been equalized when I_{ht} changes. In iterative optimization, the joint action and mutual influence

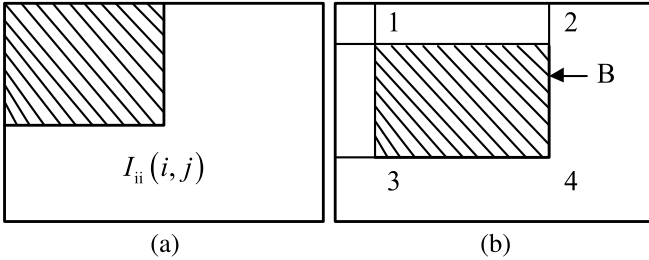


Fig. 4. (a) Example of an integral image. (b) Operation flowchart of an integral image.

of I_{ht} and I_{dt} are mainly reflected as:

$$\begin{aligned} I_{HE} &= I_{HE}^{\text{Left}} \cup I_{HE}^{\text{Right}}, \\ I_{HE}^{\text{Left}}(T) &= (I_{dt} - I_{\min}) \times \text{CDF}(T) + I_{\min}, \\ T &\in [0, I_{ht}], \\ I_{HE}^{\text{Right}}(T) &= (I_{\max} - I_{dt}) \times \text{CDF}(T) + I_{dt}, \\ T &\in [I_{ht} + 1, L - 1], \end{aligned} \quad (10)$$

where I_{\max} and I_{\min} represent the maximum and minimum gray levels, and $\text{CDF}()$ represents the cumulative distribution function of the histogram. Via the above solution scheme, we maximize the information entropy of the total histogram to obtain the best threshold I_{best} of the dynamic range threshold I_{dt} . We obtain the global contrast enhanced underwater image I_{GE} from the color-corrected underwater image when the image information entropy after equalizing the two histograms is maximum.

D. Optimized Local Contrast

In this section, we aim to improve the local contrast of the color-corrected image using the fast integration optimized local contrast enhancement strategy. The global contrast optimization strategy ignores the local contrast enhancement of the image, so the local contrast enhancement has a positive effect on the quality improvement of underwater images. We consider that the luminance and color channels are independent in the CIELAB color model, so we first convert the color-corrected underwater image from the RGB color model to the CIELAB color model. Meanwhile, we employ different correction strategies in different channels.

Bi-histogram [17], [36] has an obvious advantage in global contrast enhancement but cannot effectively enhance local contrast. Recently, the full use of local feature information has gradually established effectiveness in local contrast enhancement [9], [37]. Inspired by the local contrast method [9], we employ an integral image to quickly count the mean values of the local blocks of the image. Meanwhile, we fully utilize these local mean values to enhance the local contrast of the color-corrected image. For the luminance channel L , we first count its local integral image. As shown in Fig. 4 (a), the sum of gray pixel values in the oblique area of the luminance channel represents any pixel coordinate of the integral image, which is expressed as:

$$L_{ii}(i, j) = \sum_{i' \leq i, j' \leq j} L(i', j'), \quad (11)$$

where $L(i', j')$ represents the integral image, which can be solved iteratively using Eqs. (12) and (13):

$$L_{\text{Col}}(i, j) = L_{\text{Col}}(i, j - 1) + L(i, j), \quad (12)$$

$$L_{ii}(i, j) = L_{ii}(i - 1, j) + L_{\text{Col}}(i, j), \quad (13)$$

where $L_{\text{Col}}(i, j)$ represents the integral value of a column, $L_{\text{Col}}(i, -1) = 0$ and $L_{ii}(-1, j) = 0$. The integration image for each local block of the luminance channel can be obtained by traversing it only once, so the computational complexity is low. As shown in Fig. 4 (b), the total number of grey pixels in the shaded local block can be calculated quickly from the values taken at positions 1, 2, 3, and 4 in the integral image, i.e., the total number of grey pixels in the local block, and the calculation of the integral image is independent of the size of the local window.

Taking local image block B as an example, we assume that the vertex coordinate of the upper left corner of the image block is (i, j) , its width is M and height is N , and the gray matrix is $L_B(i, j)$. The gray mean value of the local block is:

$$u_B = \frac{\sum_{y=j}^{j+M-1} \sum_{x=i}^{i+N-1} L_B(x, y)}{(M \times N)}, \quad (14)$$

where $\sum_{y=j}^{j+M-1} \sum_{x=i}^{i+N-1} L_B(x, y)$ is the sum of the total pixel values of the local block, the grey mean values of a local block can be calculated from the integral image, thus avoiding the need for window traversal and increasing the speed of solving for the grey mean values. The strategy can reduce the computational complexity of the local mean from $O(n^2)$ to $O(1)$. We employ the mean value of local image blocks to enhance the contrast of the luminance channel. Low-frequency components in an image usually represent flatter areas of the image, and high-frequency components in an image typically represent edges and textures in the image.

In local contrast enhancement, we approximate the mean value of the local image block as the low-frequency component and subtract the low-frequency component from the original local image block to obtain the high-frequency component. In practice, the high-frequency component is enhanced appropriately to get a high-quality image. Therefore, an enhancement control factor is introduced in this section to adjust the enhancement degree of high-frequency components adaptively. For simplicity, take the enhancement process of any point in local image block B as an example, and the enhancement process can be defined as:

$$L_{BE}(x, y) = u_B + \beta \times (L_B(x, y) - u_B), \quad (15)$$

where β is the factor controlling the local contrast enhancement of the image. Extensive analysis of statistical results shows that β is set between 2 and 2.5, which has good enhancement performance. In our work, β is set to 2.1. For heavily attenuated underwater images, more than the use of attenuation map guided color correction alone is required to solve the color distortion problem completely. For color channels a and b , we first utilize Eq. (2) to calculate the mean pixel values \bar{I}_a and \bar{I}_b of color channels a and b . If $a > b$,

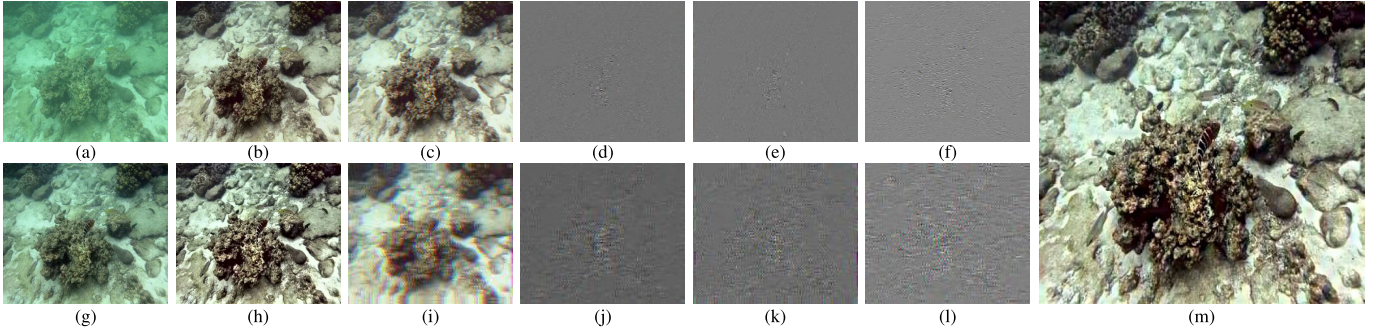


Fig. 5. **Raw underwater image and its corresponding results for each core step.** From left to right are (a) Raw underwater image, (b) Global contrast-enhanced image, (c) Approximate low-frequency component, (d) Vertical high-frequency component, (e) Horizontal high-frequency component, (f) Diagonal high-frequency component, (g) Color corrected image, (h) Local contrast-enhanced image, (i) Approximate low-frequency component, (j) Vertical high-frequency component, (k) Horizontal high-frequency component, (l) Diagonal high-frequency component, (m) Enhanced underwater image, respectively.

we perform $I_{bc} = I_b + (\bar{I}_a - \bar{I}_b) \times I_b$ to correct the b channel. In contrast, we perform $I_{ac} = I_a + (\bar{I}_b - \bar{I}_a) \times I_a$ to correct the b channel. Finally, we converted the underwater image from the CIELAB color model to the RGB color model to obtain a local contrast-enhanced underwater image I_{LE} .

E. Weighted Wavelet Fusion

Traditional fusion methods [9], [16], [40] rely on multiple feature maps to integrate different enhanced versions to obtain a high-quality underwater image, but too many features make the robustness of the algorithm challenging and the effectiveness of these feature maps varies widely. Unlike these fusion methods, we employ a weighted wavelet visual perception fusion strategy to integrate high- and low-frequency components of different scales to obtain a high-quality underwater image. Wavelet transform [65] has the characteristics of multi-resolution, multi-scale and multi-temporal, which has been widely used in image compression, denoising, and fusion. The wavelet transform of an image can be expressed as:

$$W_\varphi(k, m, n) = \frac{\sum_{x=0}^{M-1} \sum_{y=0}^{N-1} I(x, y) \varphi_{k, m, n}(x, y)}{\sqrt{M \times N}}, \quad m, n = 0, 1, 2, \dots, 2^j - 1, \quad (16)$$

$$W_{\varphi'}(k, m, n) = \frac{\sum_{x=0}^{M-1} \sum_{y=0}^{N-1} I(x, y) \phi'_{k, m, n}(x, y)}{\sqrt{M \times N}}, \quad k \in \{V, H, D\}, \quad (17)$$

where $W_\varphi(k, m, n)$ is the approximate coefficient, $W_{\varphi'}(k, m, n)$ is the detail coefficient, I is an input image of size $M \times N$, $\varphi(x, y)$ is a 2-dimensional Gaussian function, and $\phi(x, y)$ is a 2-dimensional wavelet function. For the global and local contrast-enhanced underwater images, we first obtain the approximate low-frequency component and the vertical, horizontal, and diagonal high-frequency components of each enhanced version by first-order wavelet transform, they are defined as I_{Alf} , I_{Vlf} , I_{Hlf} , and I_{Dlf} , respectively. As shown in Fig. 2, we utilize the wavelet decomposition strategy to decompose each component into a four-layer pyramid by a down-sampling operation.

Wavelet decomposition is used to extract the low-frequency and high-frequency components from various enhanced image

versions. The low-frequency components carry the primary information and structural elements of the image, while the high-frequency components contain the finer details. Therefore, the wavelet inverse transform is used for upsampling the decomposed low and high-frequency components to reconstruct an enhanced underwater image, which can be expressed as:

$$I_E = \sum_l U_d(WIT_l(I_{Alf}^l, I_{Vlf}^l, I_{Hlf}^l, I_{Dlf}^l)), \quad (18)$$

where $WIT_l()$ is the wavelet inverse transform function, U_d is the upsampling operator with factor $d = 2^{l-1}$, l is the number of layer in the wavelet pyramid, and I_E is the enhanced underwater image. Unfortunately, the above equation does not adequately consider enhancing the high-frequency component. Therefore, we introduce a weighted factor for each high-frequency component to improve the texture detail of the image. The average gradient is a metric for assessing the level of detail in an image. A higher value indicates that the image contains more details, and it is defined as:

$$\nabla G = \frac{\sum_{i=1}^{M-1} \sum_{j=1}^{N-1} \sqrt{(dx(i, j))^2 + (dy(i, j))^2}}{(M-1)(N-1)}. \quad (19)$$

In our work, we use the average gradient to design the weighting factors. ∇G_{VH} , ∇G_{HH} , and ∇G_{DH} represent the average gradient of the vertical, horizontal, and diagonal components of the reconstructed image, respectively. λ_{VH} , λ_{HH} , and λ_{DH} represent the weight factor of the vertical, horizontal, and diagonal components of the reconstructed image, respectively. They are defined as:

$$\lambda_V = 1 + \frac{\nabla G_{VH}}{\nabla G_{VH} + \nabla G_{HH} + \nabla G_{DH}}, \quad (20)$$

$$\lambda_H = 1 + \frac{\nabla G_{HH}}{\nabla G_{VH} + \nabla G_{HH} + \nabla G_{DH}}, \quad (21)$$

$$\lambda_D = 1 + \frac{\nabla G_{DH}}{\nabla G_{VH} + \nabla G_{HH} + \nabla G_{DH}}. \quad (22)$$

We designed the weighted wavelet fusion using the gradient calculation Eq. (19) and the weight calculation Eqs. (20), (21), and (22), it is expressed as:

$$I_{FE} = \sum_l U_d(WIT_l(\lambda_V I_{Alf}^l, \lambda_H I_{Vlf}^l, I_{Hlf}^l, \lambda_D I_{Dlf}^l)), \quad (23)$$

where I_{FE} is the final enhanced underwater image obtained by weighted wavelet-aware fusion. Fig. 5 demonstrates the results of each essential step. It can observe that the enhanced underwater image has a satisfying visual result. Specifically, the image with a natural appearance, high contrast, and precise texture details.

IV. EXPERIMENT AND ANALYSIS

In this section, we implement extensive quantitative and qualitative evaluations on several standard datasets to evaluate the performance of our proposed WWPF method. Subsequently, we perform the analysis of detail enhancement, ablation studies, application tests, and generalization performance. Due to limited space, most experimental results can be found in the supplementary material.

Compared Methods: We compared our WWPF with ten methods, including three image restoration methods (GDCP [26], DTVR [6], GIFM [31]), three image enhancement methods (CBAF [16], BRUE [33], ADCE [38]), and four deep learning methods (FUNIE-GAN [53], UIEC²-Net [50], PUIE-Net [55], SGUIE-Net [2]). Since the source code of CBAF [16] is not publicly available, we used the code¹ reproduced by other authors. For the GDCP [26], DTVR [6], GIFM [31], BRUE [33], ADCE [38], FUNIE-GAN [53], UIEC²-Net [50], PUIE-Net [55], and SGUIE-Net [2] methods, we used the codes released by the authors to output their results.

Benchmark Datasets: UCCS [14], UIQS [14], and UIEB [15] three datasets are selected to test the enhanced performance of our WWPF method. UCCS [14] includes three 100-images subsets of bluish, blue-green, and greenish tones, and it is primarily utilized to evaluate the performance of different methods for color correction of underwater images. UIQS [14] includes 726-images subsets of A, B, C, D, and E degradation levels, which is used to evaluate the visibility enhancement performance of different methods for underwater images. UIEB [15] includes 890 underwater images with different degradation scenes, which is used to evaluate the enhancement performance of different methods for underwater images.

Evaluation Metrics: We employ five commonly-used image quality evaluation metrics to evaluate the enhancement performance of different methods quantitatively, and they are average gradient (AG) [36], information entropy (IE) [64], edge intensity (EI) [36], underwater color image quality evaluation metric (UCIQE) [66], and colorfulness contrast fog density index (CCF) [67]. A higher AG [36] score means better image clarity. A higher IE [64] score means the richer the information of the image. A higher EI [36] score means a clearer texture of the image. A higher UCIQE [66] or CCF [67] scores mean a better human visual perception. Please note that the scores of UCIQE and CCF do not accurately reflect the performance of underwater image enhancement methods in some cases.

¹<https://github.com/bilityniu/underimage-fusion-enhancement>

A. Evaluation on the UCCS Dataset

1) Qualitative Comparisons: For underwater image quality evaluation, the ability to correct color distortion is the primary task to evaluate the performance of different methods. We first evaluate the color correction capabilities of different methods for the UCCS dataset. In Fig. 6 (a), the various color distortion significantly hampers the structural detail of the underwater scene. In terms of color correction, GDCP [26], DTVR [6], and GIFM [31] obtain unsatisfactory color correction performance. BRUE [33], CBAF [16], FUNIE-GAN [53], and SGUIE-Net [2] introduce unwanted color distortions, such as reddish, yellow, blue artifacts, etc. ADCE [38], UIEC²-Net [50], and PUIE-Net [55] have good color correction capacity for underwater images facing various color distortions, but ADCE reduces detail and color saturation of the enhanced underwater image. UIEC²-Net [50] and PUIE-Net [55] are weaker than our WWPF method in terms of detail and contrast enhancement. In summary, our WWPF method has good correction capacity for the various color distortion issues faced by underwater images, and it also has good texture detail and contrast enhancement performance.

2) Quantitative Comparisons: Our WWPF method has good enhancement performance for color, texture detail, and contrast in terms of qualitative evaluation. Meantime, we quantitatively evaluate the advantages of our WWPF in terms of evaluation metrics. Table I reports the AG [36], IE [64], EI [36], UCIQE [66], and CCF [67] scores of different methods tested on the UCCS [14] dataset. From Table I, we can observe that our WWPF method has the highest or approximately the highest scores of AG [36], IE [64], EI [36], UCIQE [66], and CCF [67], which also proves that our WWPF method also has good results in the quantitative evaluation. To sum up, our method has good qualitative and quantitative results for the UCCS dataset.

B. Evaluation on the UIQS Dataset

1) Qualitative Comparisons: We further qualitatively compare the performance of different methods tested on the UIQS [14] dataset for visibility enhancement of underwater images with different degradation levels. In Fig 7, we see that most of the methods positively improve the visibility of underwater degraded images from UIQS [17]. In terms of color correction, GDCP [26], DTVR [6], GIFM [31], FUNIE-GAN [53], and SGUIE-Net [2] cannot effectively correct color distortion. CBAF [16], BRUE [33], and ADCE [38] introduce local artifacts and reddish halos for some cases. UIEC²-Net [50], PUIE-Net [55], and our WWPF all have satisfactory color correction results. In terms of contrast enhancement, GDCP [26], DTVR [6], GIFM [31], FUNIE-GAN [53], and SGUIE-Net [2] are weaker than UIEC²-Net [50] and PUIE-Net [55]. Although CBAF [16], BRUE [33], and ADCE [38] are superior to UIEC²-Net [50] and PUIE-Net [55] in contrast improvement. However, CBAF [16], BRUE [33], and ADCE [38] may introduce local artifacts or lose texture details. Satisfactorily, our WWPF method outperforms the above methods regarding color correction, contrast enhancement, and detail sharpening.

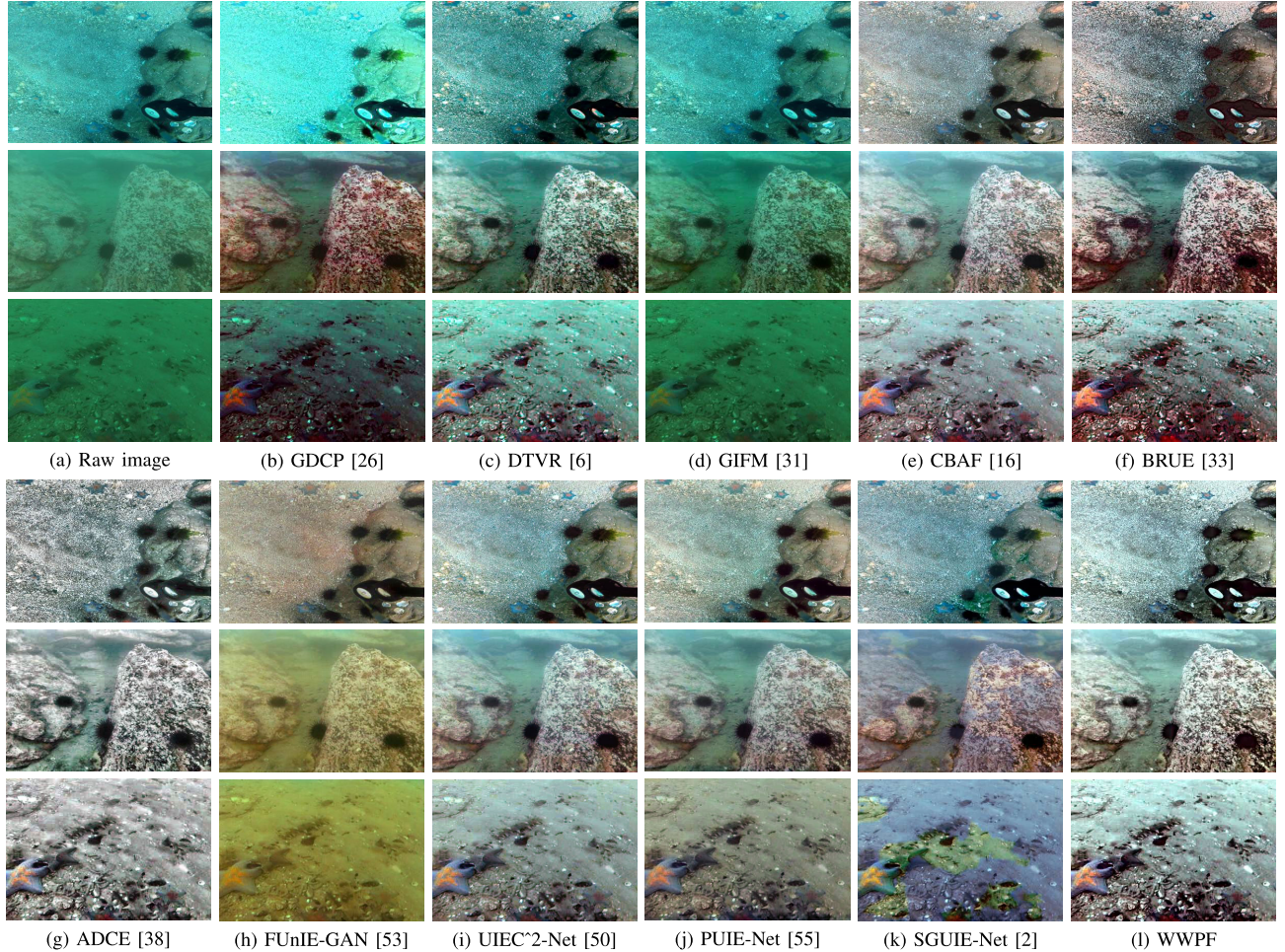


Fig. 6. Visual comparisons on three underwater images with color casts sampled from the UCCS [14] dataset. From top to bottom are samples of blue, blue-green, and green distorted underwater images.

TABLE I

QUANTITATIVE EVALUATION SCORES OF OUR WWPF METHOD WITH THE COMPARED METHODS TESTED ON THE UCCS [14], UIQS [14], AND UIEB [15] DATASETS. THE HIGHEST QUANTITATIVE SCORES ARE MARKED IN RED, WHILE THE SECOND-HIGHEST SCORES ARE MARKED IN BLUE

Methods	UCCS [14]				UIQS [14]				UIEB [15]				Mean			
	AG↑	IE↑	EI↑	UCIQE↑	CCF↑	AG↑	IE↑	EI↑	UCIQE↑	CCF↑	AG↑	IE↑	EI↑	UCIQE↑	CCF↑	
GDCP [26]	5.604	7.158	55.549	0.540	24.821	5.732	7.145	57.687	0.540	21.805	5.604	7.158	55.549	0.540	24.821	18.684
DTVR [6]	7.547	7.660	75.368	0.583	32.956	7.917	7.545	79.930	0.592	31.717	7.547	7.660	75.368	0.608	32.956	25.064
GIFM [31]	3.583	7.334	35.991	0.494	23.624	3.916	7.352	40.728	0.524	22.407	5.119	7.426	50.635	0.567	26.621	15.755
CBAF [16]	6.564	7.632	64.990	0.580	20.746	6.721	7.596	67.332	0.582	20.683	6.564	7.632	64.990	0.580	20.746	20.263
BRUE [33]	9.886	7.783	97.087	0.585	30.360	10.090	7.755	100.51	0.594	30.643	9.886	7.783	97.087	0.593	30.360	29.400
ADCE [38]	9.276	7.668	92.337	0.527	26.976	9.394	7.652	94.917	0.528	26.814	9.276	7.668	92.337	0.527	26.976	27.525
FUNIE-GAN [53]	3.711	7.420	37.913	0.497	16.449	3.748	7.434	38.705	0.510	17.834	3.711	7.420	37.913	0.497	16.449	13.347
UIEC^2-Net [50]	5.708	7.586	56.804	0.562	19.709	6.013	7.580	60.726	0.568	20.228	5.708	7.586	56.804	0.562	19.709	18.390
PUIE-Net [55]	4.913	7.506	49.444	0.526	19.560	5.242	7.423	53.473	0.538	20.521	6.044	7.583	60.040	0.581	21.595	17.666
SGUIE-Net [2]	5.641	7.595	56.552	0.560	23.706	5.836	7.521	59.405	0.565	23.614	7.451	7.670	74.102	0.614	31.662	20.833
WWPF	9.403	7.806	93.557	0.588	34.750	9.909	7.785	99.796	0.595	36.767	10.818	7.684	105.982	0.617	40.851	31.127

2) *Quantitative Comparisons:* Table I reports shows the AG [36], IE [64], EI [36], UCIQE [66], and CCF [67] scores of different method experiments on the UIQS [14] dataset. As shown in Table I, our WWPF method has the highest or approximately the highest score for the quantitative evaluation of the entire UIQS [14] dataset. Overall, our WWPF method has better results than the compared methods for qualitative and quantitative evaluation of underwater images with different degradation levels.

C. Evaluation on the UIEB Dataset

1) *Qualitative Comparisons:* To further evaluate the enhancement performance of our WWPF method for different

degradation types of underwater images, our method is compared quantitatively to other methods on the UIEB [15] dataset. As shown in Fig. 8 (a), we selected green-distorted, blue-distorted, and blurred underwater images to comprehensively evaluate the enhanced performance of our WWPF method. For green-distorted underwater image, GDCP [26], GIFM [31], and FUNIE-GAN [53] fail in color correction. DTVR [6], ADCE [38], and PUIE-Net [55] introduce local artifacts and the color correction results are unsatisfactory. Although CBAF [16], BRUE [33], UIEC^2-Net [50], and SGUIE-Net [2] can correct green distortion well, they all introduce slightly red distortion. Our WWPF method can remove the green distortion better without introducing an additional

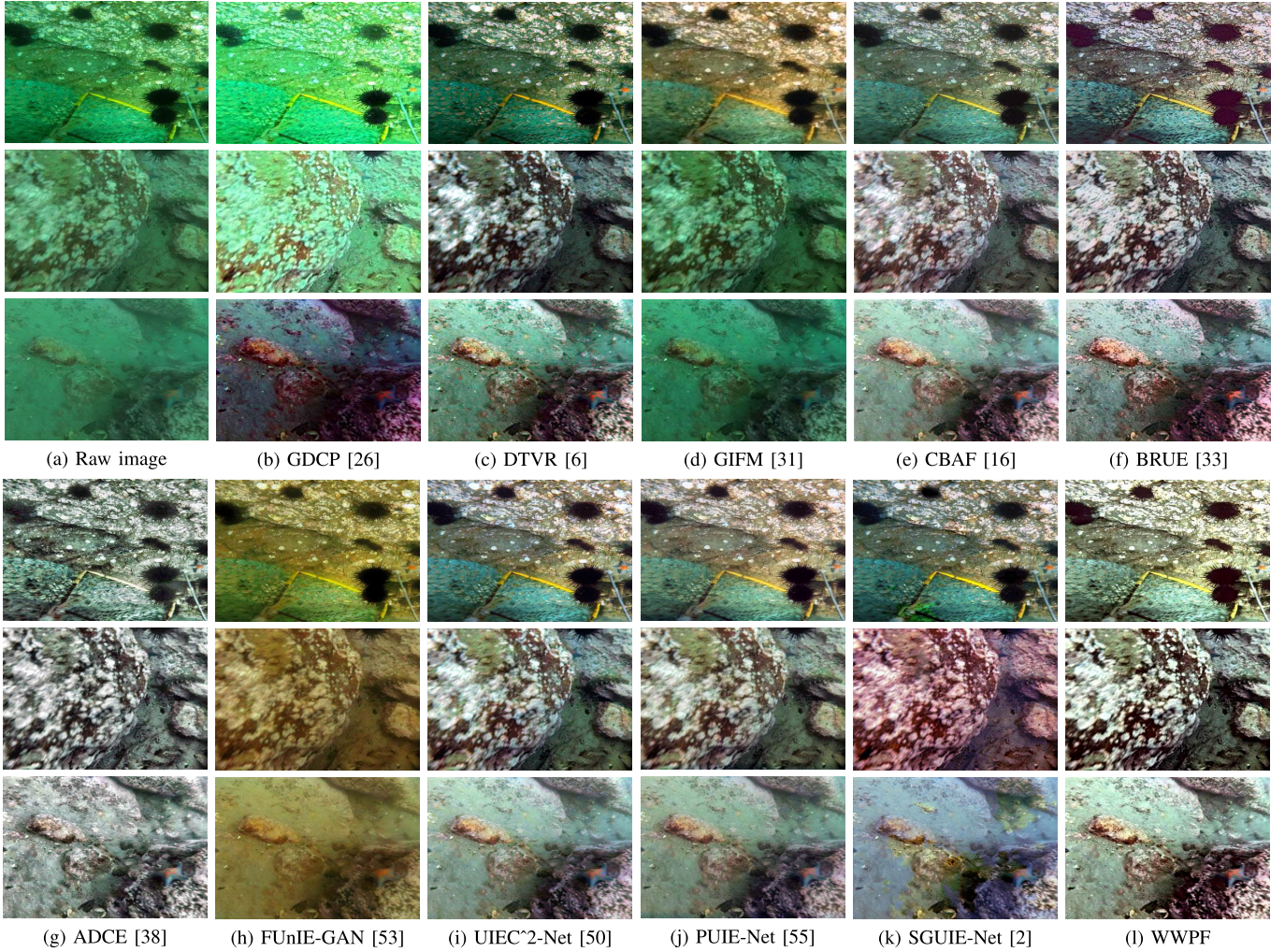


Fig. 7. Visual comparisons on underwater images with different levels of degradation sampled from the UIQS [14] dataset. From top to bottom are samples of underwater images with quality levels A, C, and D.

reddish appearance. For blue-distorted underwater image, GDCP [26], DTVR [6], GIFM [31], and FUnIE-GAN [53] exacerbate the color distortion issue. CBAF [16], UIEC²-Net [50], and PUIE-Net [55] cannot correct the blue distortion in the background area well. BRUE [33], ADCE [38], and SGUIE-Net [2] have good color correction results, but they are weaker than our WWPF in texture detail and contrast enhancement. For blurred underwater image, the deblurring ability of GDCP [26], FUnIE-GAN [53], PUIE-Net [55], and SGUIE-Net [2] is unsatisfactory. GIFM [31], CBAF [16], BRUE [33], and UIEC²-Net [50] have a good deblurring effect, but their enhancement of texture details is insufficient. DTVR [6] introduces the overexposure problem, ADCE [38] loses texture details, while our WWPF has better deblurring and texture detail enhancement performance.

2) *Quantitative Comparisons*: Table I reports the AG [36], IE [64], EI [36], UCIQE [66], and CCF [67] scores of different methods tested on the UIEB [15] dataset. From Table I, we can observe that our WWPF achieved the best or approximately the best quantitative score. In addition, our WWPF has the highest overall mean quantitative score for the UCCS [14], UIQS [14], and UIEB [15] datasets. Overall, our WWPF

achieves good qualitative and quantitative results for the three standard datasets.

D. Evaluation of Detail Enhancement

Underwater images with sharp textural details are significant for high-level drive tasks in underwater vision [68]. Fig. 9 shows zoomed-in regions of a representative underwater image enhanced by different methods to evaluate the performance of detail enhancement. From a global perspective, our WWPF method has better performance in color correction, contrast enhancement and detail sharpening. From a local perspective, our WWPF method can significantly improve the texture details and color information of the amplified areas of the blue and red boxes in Fig. 9.

E. Ablation Study

To comprehensively demonstrate the positive impact of each core module in our WWPF method on enhanced results, we performed the following ablation analyses on the UCCS [14], UIQS [14], and UIEB [15] datasets, including (a) our WWPF method without attenuation map guided color

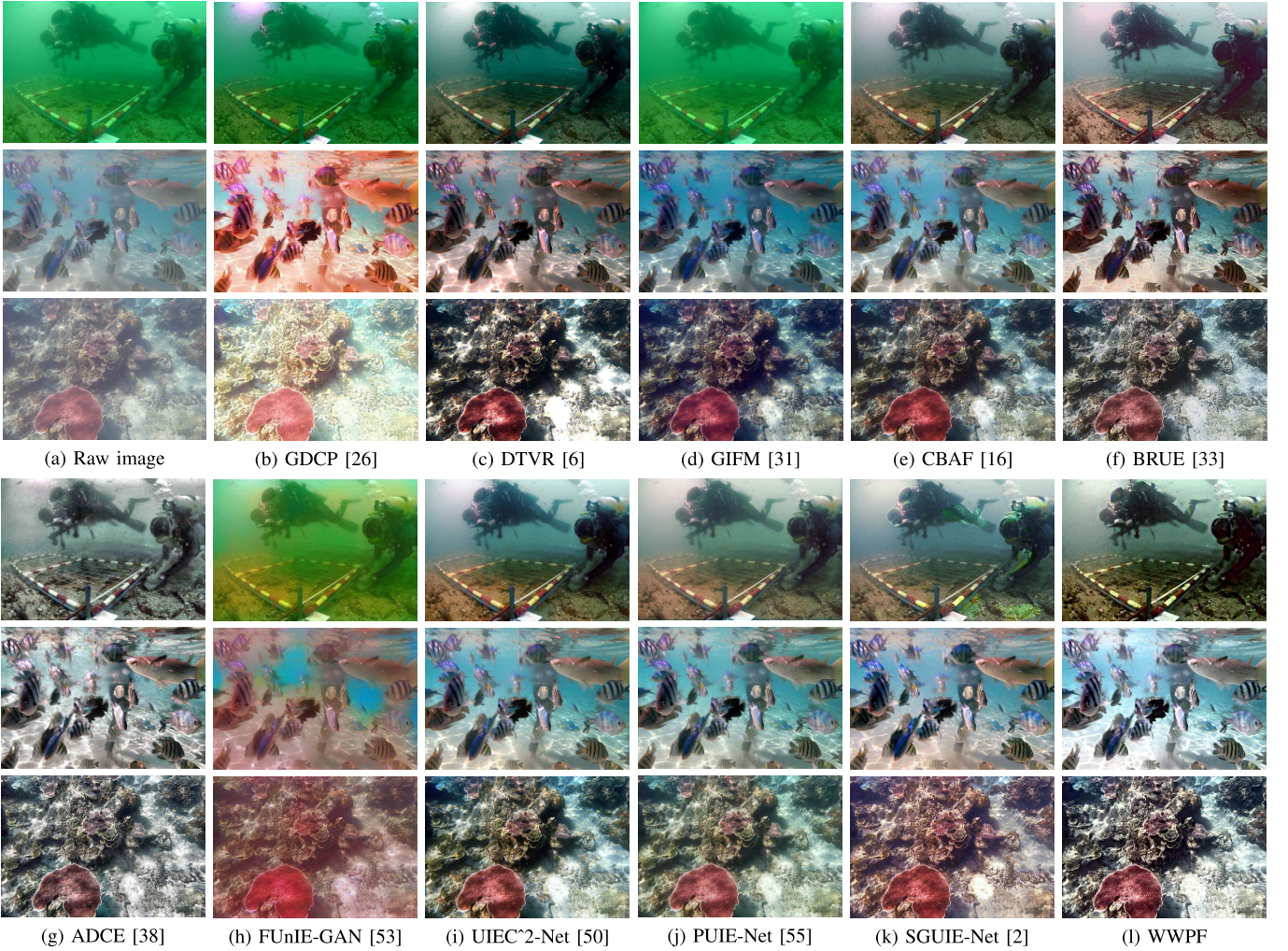


Fig. 8. Visual comparisons on underwater images of different degradation types sampled from the UIEB dataset [15]. From top to bottom are green-distorted, blue-distorted, and blurred underwater images.

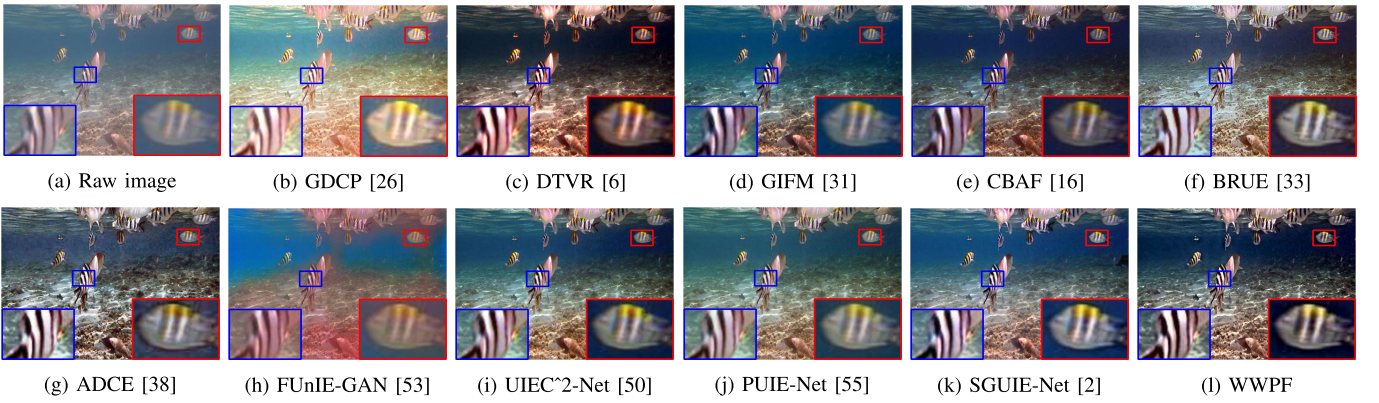


Fig. 9. Texture detail enhancement comparisons on a typical underwater image with bluish and low visibility sampled from the UIEB [15] dataset.

correction (-w/o AMGCC), (b) our WWPF method without optimized global contrast (-w/o OGC), (c) our WWPF method without optimized local contrast (-w/o OLC), (d) our WWPF method without weighted wavelet fusion (-w/o WWF).

Fig. 10 reports the visual results of our WWPF method testing on the UCCS [14], UIQS [14], and UIEB [15] datasets. The visual results shown in Fig. 10 can be observed as follows:

- 1) -w/o AMGCC improves underwater image visibility but fails in color correction and local contrast enhancement;
- 2) -w/o OGC shows excellent performance in local contrast enhancement, but it needs to be improved in global contrast enhancement;
- 3) -w/o OLC show effectiveness in global contrast enhancement but lack performance in local contrast enhancement;
- 4) -w/o WWF fails in the fusion of global and

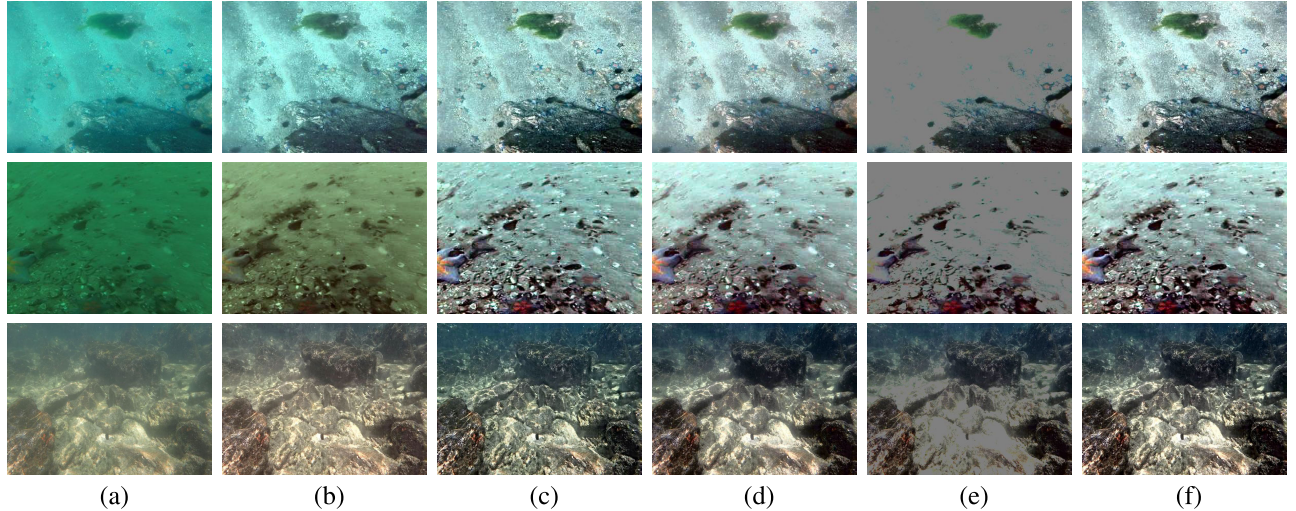


Fig. 10. Ablation results of each core module of our WWPF method test on the UCCS [14], UIQS [14], and UIEB [15] datasets. (a) Raw underwater images. (b) -w/o AMGCC. (c) -w/o OGC. (d) -w/o OLC. (e) -w/o WWF. (f) WWPF (full model).

TABLE II

ABLATION STUDIES OF DIFFERENT MODULES TESTED ON THE UCCS [14], UIQS [14], AND UIEB [15] DATASETS. THE HIGHEST QUANTITATIVE SCORES ARE MARKED IN RED, WHILE THE SECOND-HIGHEST SCORES ARE MARKED IN BLUE

Ablated models	UCCS [14]					UIQS [14]					UIEB [15]				
	AG↑	IE↑	EI↑	UCIQE↑	CCF↑	AG↑	IE↑	EI↑	UCIQE↑	CCF↑	AG↑	IE↑	EI↑	UCIQE↑	CCF↑
-w/o AMGCC	5.455	7.248	53.540	0.465	18.294	6.013	7.282	60.171	0.487	20.798	8.655	7.523	84.500	0.573	33.096
-w/o OGC	9.461	7.709	93.986	0.575	29.072	9.887	7.692	99.469	0.581	29.838	10.844	7.666	104.163	0.609	34.281
-w/o OLC	6.761	7.795	67.395	0.577	29.367	6.955	7.032	70.925	0.583	30.425	7.861	7.732	77.005	0.608	33.539
-w/o WWF	3.343	3.944	33.903	0.454	19.191	3.772	4.208	38.477	0.458	21.561	4.874	4.876	48.027	0.479	24.835
WWPF (full model)	9.403	7.806	93.557	0.588	34.750	9.909	7.785	99.796	0.595	36.767	10.818	7.684	105.982	0.617	40.851

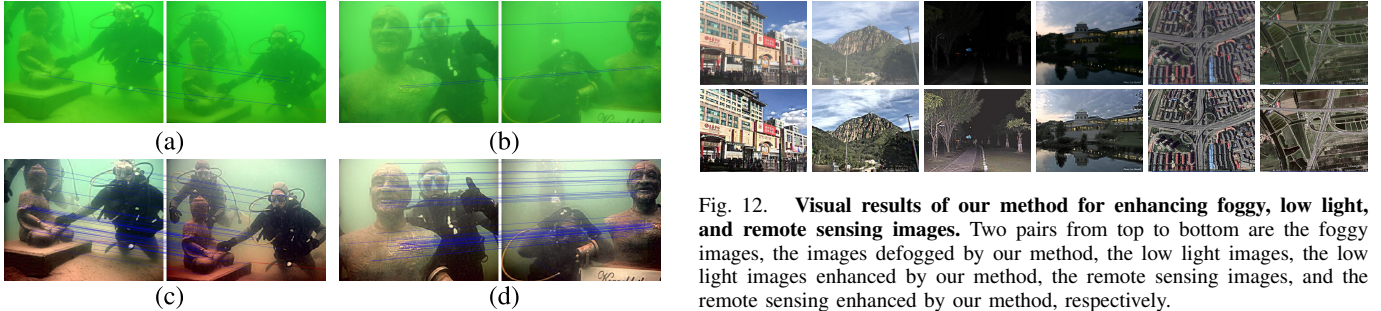


Fig. 11. Examples of key feature point matching before and after underwater images are enhanced. (a) and (b) represent the matching results of key feature points of the raw underwater image pairs. (c) and (d) represent the key feature point matching results of the raw underwater image pairs enhanced by our method.

local contrast-enhanced images and cannot effectively enhance the contrast of the result; and 5) Our full model can achieve satisfactory visual results.

Table II reports the AG [36], IE [64], EI [36], UCIQE [66], and CCF [67] scores for each core module of our WWPF method tested on the UCCS [14], UIQS [14], and UIEB [15] datasets. From Table II, we can observe that our full model has optimal or suboptimal scores in most cases. The ablation study qualitatively and quantitatively demonstrated that each core module positively impacts the final enhancement result.

F. Applications

High-quality underwater image is of great significance for further analysis and application of the underwater image.



Fig. 12. Visual results of our method for enhancing foggy, low light, and remote sensing images. Two pairs from top to bottom are the foggy images, the images defogged by our method, the low light images enhanced by our method, the remote sensing images, and the remote sensing enhanced by our method, respectively.

Therefore, we use the SIFT operator to calculate the matching number of key feature points before and after the underwater image is enhanced. Fig. 11 reports the matching numbers of specific key feature points. The number of feature point matching in Fig. 11 (a) is 4, and the number of feature point matching in the corresponding enhanced image is 55. The number of feature point matching in Fig. 11 (b) is 3, and the number of feature point matching in the corresponding enhanced image is 46. In general, the number of key feature points in underwater images enhanced by our method is significantly increased.

G. Generalization Performance of Our Method

To further evaluate the enhancement performance of our WWPF for other low-level visual tasks, we tried to enhance other low-visibility images in Fig. 12. From Fig. 12, it can observe that our WWPF method has better enhancement

performance for fog, low light, and remote sensing images without any parameter fine-tuning. Therefore, it can also be shown that our WWP has good generalization performance for other low-level visual tasks without parameter fine-tuning.

V. CONCLUSION

We describe in detail the proposed underwater image enhancement method. Our method mainly includes color correction, optimization of global and local contrast, and weighted wavelet of different enhanced versions of underwater images. We utilize weighted wavelet fusion to make up for the advantages of global contrast, local contrast, and texture details between images of different enhanced versions. Qualitative and quantitative evaluations demonstrated the superior enhancement capabilities and good generalization performance of our WWPF on three standard datasets. Compared with most existing methods, although our WWPF outputs satisfactory results, it can not suppress image noise well. Therefore, we will explore how to effectively suppress noise without affecting the enhanced performance of our WWPF method in future work.

REFERENCES

- [1] C. Fu et al., "Rethinking general underwater object detection: Datasets, challenges, and solutions," *Neurocomputing*, vol. 517, pp. 243–256, Jan. 2023.
- [2] Q. Qi, K. Li, H. Zheng, X. Gao, G. Hou, and K. Sun, "SGUIE-Net: Semantic attention guided underwater image enhancement with multi-scale perception," *IEEE Trans. Image Process.*, vol. 31, pp. 6816–6830, 2022.
- [3] H. Lu, Y. Li, T. Uemura, H. Kim, and S. Serikawa, "Low illumination underwater light field images reconstruction using deep convolutional neural networks," *Future Gener. Comput. Syst.*, vol. 82, pp. 142–148, May 2018.
- [4] W. Zhang, L. Dong, T. Zhang, and W. Xu, "Enhancing underwater image via color correction and Bi-interval contrast enhancement," *Signal Process., Image Commun.*, vol. 90, Jan. 2021, Art. no. 116030.
- [5] L. Chen et al., "Perceptual underwater image enhancement with deep learning and physical priors," *IEEE Trans. Circuits Syst. Video Technol.*, vol. 31, no. 8, pp. 3078–3092, Aug. 2021.
- [6] X. Ding, Z. Liang, Y. Wang, and X. Fu, "Depth-aware total variation regularization for underwater image dehazing," *Signal Process., Image Commun.*, vol. 98, Oct. 2021, Art. no. 116408.
- [7] J. Xie, G. Hou, G. Wang, and Z. Pan, "A variational framework for underwater image dehazing and deblurring," *IEEE Trans. Circuits Syst. Video Technol.*, vol. 32, no. 6, pp. 3514–3526, Jun. 2022.
- [8] H. Song, L. Chang, Z. Chen, and P. Ren, "Enhancement-Registration-Homogenization (ERH): A comprehensive underwater visual reconstruction paradigm," *IEEE Trans. Pattern Anal. Mach. Intell.*, vol. 44, no. 10, pp. 6953–6967, Oct. 2022.
- [9] W. Zhang, L. Dong, and W. Xu, "Retinex-inspired color correction and detail preserved fusion for underwater image enhancement," *Comput. Electron. Agricult.*, vol. 192, Jan. 2022, Art. no. 106585.
- [10] H. Wang, S. Sun, and P. Ren, "Meta underwater camera: A smart protocol for underwater image enhancement," *ISPRS J. Photogramm. Remote Sens.*, vol. 195, pp. 462–481, Jan. 2023.
- [11] C. Li, S. Anwar, J. Hou, R. Cong, C. Guo, and W. Ren, "Underwater image enhancement via medium transmission-guided multi-color space embedding," *IEEE Trans. Image Process.*, vol. 30, pp. 4985–5000, 2021.
- [12] Z. Jiang, Z. Li, S. Yang, X. Fan, and R. Liu, "Target oriented perceptual adversarial fusion network for underwater image enhancement," *IEEE Trans. Circuits Syst. Video Technol.*, vol. 32, no. 10, pp. 6584–6598, Oct. 2022.
- [13] Z. Huang, J. Li, Z. Hua, and L. Fan, "Underwater image enhancement via adaptive group attention-based multiscale cascade transformer," *IEEE Trans. Instrum. Meas.*, vol. 71, pp. 1–18, 2022.
- [14] R. Liu, X. Fan, M. Zhu, M. Hou, and Z. Luo, "Real-world underwater enhancement: Challenges, benchmarks, and solutions under natural light," *IEEE Trans. Circuits Syst. Video Technol.*, vol. 30, no. 12, pp. 4861–4875, Dec. 2020.
- [15] C. Li et al., "An underwater image enhancement benchmark dataset and beyond," *IEEE Trans. Image Process.*, vol. 29, pp. 4376–4389, 2020.
- [16] C. O. Ancuti, C. Ancuti, C. De Vleeschouwer, and P. Bekaert, "Color balance and fusion for underwater image enhancement," *IEEE Trans. Image Process.*, vol. 27, no. 1, pp. 379–393, Jan. 2018.
- [17] W. Zhang, X. Pan, X. Xie, L. Li, Z. Wang, and C. Han, "Color correction and adaptive contrast enhancement for underwater image enhancement," *Comput. Electr. Eng.*, vol. 91, May 2021, Art. no. 106981.
- [18] Q. Jiang, Y. Gu, C. Li, R. Cong, and F. Shao, "Underwater image enhancement quality evaluation: Benchmark dataset and objective metric," *IEEE Trans. Circuits Syst. Video Technol.*, vol. 32, no. 9, pp. 5959–5974, Sep. 2022.
- [19] X. Fu and X. Cao, "Underwater image enhancement with global-local networks and compressed-histogram equalization," *Signal Process., Image Commun.*, vol. 86, Aug. 2020, Art. no. 115892.
- [20] C. Li, J. Guo, C. Guo, R. Cong, and J. Gong, "A hybrid method for underwater image correction," *Pattern Recognit. Lett.*, vol. 94, pp. 62–67, Jul. 2017.
- [21] Z. Liang, X. Ding, Y. Wang, X. Yan, and X. Fu, "GUDCP: Generalization of underwater dark channel prior for underwater image restoration," *IEEE Trans. Circuits Syst. Video Technol.*, vol. 32, no. 7, pp. 4879–4884, Jul. 2022.
- [22] P. L. J. Drews, E. R. Nascimento, S. S. C. Botelho, and M. F. M. Campos, "Underwater depth estimation and image restoration based on single images," *IEEE Comput. Graph. Appl.*, vol. 36, no. 2, pp. 24–35, Mar. 2016.
- [23] W. Song, Y. Wang, D. Huang, A. Liotta, and C. Perra, "Enhancement of underwater images with statistical model of background light and optimization of transmission map," *IEEE Trans. Broadcast.*, vol. 66, no. 1, pp. 153–169, Mar. 2020.
- [24] F. Xiao, F. Yuan, Y. Huang, and E. Cheng, "Turbid underwater image enhancement based on parameter-tuned stochastic resonance," *IEEE J. Ocean. Eng.*, vol. 48, no. 1, pp. 127–146, Jan. 2023.
- [25] Y. Wang, H. Liu, and L.-P. Chau, "Single underwater image restoration using adaptive attenuation-curve prior," *IEEE Trans. Circuits Syst. I, Reg. Papers*, vol. 65, no. 3, pp. 992–1002, Mar. 2018.
- [26] Y.-T. Peng, K. Cao, and P. C. Cosman, "Generalization of the dark channel prior for single image restoration," *IEEE Trans. Image Process.*, vol. 27, no. 6, pp. 2856–2868, Jun. 2018.
- [27] H.-H. Chang, C.-Y. Cheng, and C.-C. Sung, "Single underwater image restoration based on depth estimation and transmission compensation," *IEEE J. Ocean. Eng.*, vol. 44, no. 4, pp. 1130–1149, Oct. 2019.
- [28] M. Yang, A. Sowmya, Z. Wei, and B. Zheng, "Offshore underwater image restoration using reflection-decomposition-based transmission map estimation," *IEEE J. Ocean. Eng.*, vol. 45, no. 2, pp. 521–533, Apr. 2020.
- [29] D. Berman, D. Levy, S. Avidan, and T. Treibitz, "Underwater single image color restoration using haze-lines and a new quantitative dataset," *IEEE Trans. Pattern Anal. Mach. Intell.*, vol. 43, no. 8, pp. 2822–2837, Aug. 2021.
- [30] M. Muniraj and V. Dhandapani, "Underwater image enhancement by combining color constancy and dehazing based on depth estimation," *Neurocomputing*, vol. 460, pp. 211–230, Oct. 2021.
- [31] Z. Liang, W. Zhang, R. Ruan, P. Zhuang, and C. Li, "GIFM: An image restoration method with generalized image formation model for poor visible conditions," *IEEE Trans. Geosci. Remote Sens.*, vol. 60, 2022, Art. no. 4110616.
- [32] P. Zhuang, J. Wu, F. Porikli, and C. Li, "Underwater image enhancement with hyper-Laplacian reflectance priors," *IEEE Trans. Image Process.*, vol. 31, pp. 5442–5455, 2022.
- [33] P. Zhuang, C. Li, and J. Wu, "Bayesian Retinex underwater image enhancement," *Eng. Appl. Artif. Intell.*, vol. 101, May 2021, Art. no. 104171.
- [34] O. A. Aguirre-Castro et al., "Evaluation of underwater image enhancement algorithms based on Retinex and its implementation on embedded systems," *Neurocomputing*, vol. 494, pp. 148–159, Jul. 2022.
- [35] A. S. A. Ghani and N. A. M. Isa, "Automatic system for improving underwater image contrast and color through recursive adaptive histogram modification," *Comput. Electron. Agricult.*, vol. 141, pp. 181–195, Sep. 2017.

- [36] K. Z. M. Azmi, A. S. A. Ghani, Z. M. Yusof, and Z. Ibrahim, "Natural-based underwater image color enhancement through fusion of swarm-intelligence algorithm," *Appl. Soft Comput.*, vol. 85, Dec. 2019, Art. no. 105810.
- [37] W. Zhang, P. Zhuang, H.-H. Sun, G. Li, S. Kwong, and C. Li, "Underwater image enhancement via minimal color loss and locally adaptive contrast enhancement," *IEEE Trans. Image Process.*, vol. 31, pp. 3997–4010, 2022.
- [38] W. Zhang, Y. Wang, and C. Li, "Underwater image enhancement by attenuated color channel correction and detail preserved contrast enhancement," *IEEE J. Ocean. Eng.*, vol. 47, no. 3, pp. 718–735, Jul. 2022.
- [39] Y. Kang, Q. Jiang, C. Li, W. Ren, H. Liu, and P. Wang, "A perception-aware decomposition and fusion framework for underwater image enhancement," *IEEE Trans. Circuits Syst. Video Technol.*, vol. 33, no. 3, pp. 988–1002, Mar. 2023.
- [40] J. Yuan, Z. Cai, and W. Cao, "TEBCF: Real-world underwater image texture enhancement model based on blurriness and color fusion," *IEEE Trans. Geosci. Remote Sens.*, vol. 60, 2022, Art. no. 4204315.
- [41] L. Chang, H. Song, M. Li, and M. Xiang, "UIDEF: A real-world underwater image dataset and a color-contrast complementary image enhancement framework," *ISPRS J. Photogramm. Remote Sens.*, vol. 196, pp. 415–428, Feb. 2023.
- [42] T. Ren et al., "Reinforced Swin-Convs Transformer for simultaneous underwater sensing scene image enhancement and super-resolution," *IEEE Trans. Geosci. Remote Sens.*, vol. 60, 2022, Art. no. 4209616.
- [43] J. Hao, H. Yang, X. Hou, and Y. Zhang, "Two-stage underwater image restoration algorithm based on physical model and causal intervention," *IEEE Signal Process. Lett.*, vol. 30, pp. 120–124, 2023.
- [44] S. Yin, S. Hu, Y. Wang, W. Wang, C. Li, and Y.-H. Yang, "Degradation-aware and color-corrected network for underwater image enhancement," *Knowl.-Based Syst.*, vol. 258, Dec. 2022, Art. no. 109997.
- [45] C. Li, C. Guo, and C. C. Loy, "Learning to enhance low-light image via zero-reference deep curve estimation," *IEEE Trans. Pattern Anal. Mach. Intell.*, vol. 44, no. 8, pp. 4225–4238, Aug. 2022.
- [46] W. Zhang, Z. Li, H.-H. Sun, Q. Zhang, P. Zhuang, and C. Li, "SSTNet: Spatial, spectral, and texture aware attention network using hyperspectral image for corn variety identification," *IEEE Geosci. Remote Sens. Lett.*, vol. 19, pp. 1–5, 2022.
- [47] X. Fu, M. Wang, X. Cao, X. Ding, and Z.-J. Zha, "A model-driven deep unfolding method for JPEG artifacts removal," *IEEE Trans. Neural Netw. Learn. Syst.*, vol. 33, no. 11, pp. 6802–6816, Nov. 2022.
- [48] H. Lu, M. Guizani, and P.-H. Ho, "Editorial introduction to responsible artificial intelligence for autonomous driving," *IEEE Trans. Intell. Transp. Syst.*, vol. 23, no. 12, pp. 25212–25215, Dec. 2022.
- [49] X. Xue, Z. Li, L. Ma, Q. Jia, R. Liu, and X. Fan, "Investigating intrinsic degradation factors by multi-branch aggregation for real-world underwater image enhancement," *Pattern Recognit.*, vol. 133, Jan. 2023, Art. no. 109041.
- [50] Y. Wang, J. Guo, H. Gao, and H. Yue, "UIEC²-Net: CNN-based underwater image enhancement using two color space," *Signal Process., Image Commun.*, vol. 96, Aug. 2021, Art. no. 116250.
- [51] C. Li, S. Anwar, and F. Porikli, "Underwater scene prior inspired deep underwater image and video enhancement," *Pattern Recognit.*, vol. 98, Feb. 2020, Art. no. 107038.
- [52] N. Jiang, W. Chen, Y. Lin, T. Zhao, and C.-W. Lin, "Underwater image enhancement with lightweight cascaded network," *IEEE Trans. Multimedia*, vol. 24, pp. 4301–4313, 2022.
- [53] M. J. Islam, Y. Xia, and J. Sattar, "Fast underwater image enhancement for improved visual perception," *IEEE Robot. Autom. Lett.*, vol. 5, no. 2, pp. 3227–3234, Apr. 2020.
- [54] H. Wang, S. Sun, X. Bai, J. Wang, and P. Ren, "A reinforcement learning paradigm of configuring visual enhancement for object detection in underwater scenes," *IEEE J. Ocean. Eng.*, vol. 48, no. 2, pp. 443–461, Apr. 2023.
- [55] Z. Fu, W. Wang, Y. Huang, X. Ding, and K.-K. Ma, "Uncertainty inspired underwater image enhancement," in *Proc. 17th Eur. Conf. Comput. Vis. (ECCV)*, Tel Aviv, Israel, Oct. 2022, pp. 465–482.
- [56] J. Li, K. A. Skinner, R. M. Eustice, and M. Johnson-Roberson, "WaterGAN: Unsupervised generative network to enable real-time color correction of monocular underwater images," *IEEE Robot. Autom. Lett.*, vol. 3, no. 1, pp. 387–394, Jan. 2018.
- [57] Q. Qi et al., "Underwater image co-enhancement with correlation feature matching and joint learning," *IEEE Trans. Circuits Syst. Video Technol.*, vol. 32, no. 3, pp. 1133–1147, Mar. 2022.
- [58] R. Liu, Z. Jiang, S. Yang, and X. Fan, "Twin adversarial contrastive learning for underwater image enhancement and beyond," *IEEE Trans. Image Process.*, vol. 31, pp. 4922–4936, 2022.
- [59] W. Zhang, S. Jin, P. Zhuang, Z. Liang, and C. Li, "Underwater image enhancement via piecewise color correction and dual prior optimized contrast enhancement," *IEEE Signal Process. Lett.*, vol. 30, pp. 229–233, 2023.
- [60] C. O. Ancuti, C. Ancuti, C. De Vleeschouwer, and M. Sbert, "Color Channel Compensation (3C): A fundamental pre-processing step for image enhancement," *IEEE Trans. Image Process.*, vol. 29, pp. 2653–2665, 2020.
- [61] R. Protasiuk, A. Bibi, and B. Ghanem, "Local color mapping combined with color transfer for underwater image enhancement," in *Proc. IEEE Winter Conf. Appl. Comput. Vis. (WACV)*, Jan. 2019, pp. 1433–1439.
- [62] J. Yuan, W. Cao, Z. Cai, and B. Su, "An underwater image vision enhancement algorithm based on contour bougie morphology," *IEEE Trans. Geosci. Remote Sens.*, vol. 59, no. 10, pp. 8117–8128, Oct. 2021.
- [63] C. O. Ancuti, C. Ancuti, C. De Vleeschouwer, and R. Garcia, "Locally adaptive color correction for underwater image dehazing and matching," in *Proc. IEEE Conf. Comput. Vis. Pattern Recognit. Workshops (CVPRW)*, Jul. 2017, pp. 997–1005.
- [64] R. Chan, M. Rottmann, and H. Gottschalk, "Entropy maximization and meta classification for out-of-distribution detection in semantic segmentation," in *Proc. IEEE/CVF Int. Conf. Comput. Vis. (ICCV)*, Oct. 2021, pp. 5108–5117.
- [65] Y. Yu, W. Zhao, S. Li, and S. Huang, "A two-stage wavelet decomposition method for instantaneous power quality indices estimation considering interharmonics and transient disturbances," *IEEE Trans. Instrum. Meas.*, vol. 70, pp. 1–13, 2021.
- [66] M. Yang and A. Sowmya, "An underwater color image quality evaluation metric," *IEEE Trans. Image Process.*, vol. 24, no. 12, pp. 6062–6071, Dec. 2015.
- [67] Y. Wang et al., "An imaging-inspired no-reference underwater color image quality assessment metric," *Comput. Electr. Eng.*, vol. 70, pp. 904–913, Aug. 2018.
- [68] Y. Teng et al., "Multidimensional deformable object manipulation based on DN-transporter networks," *IEEE Trans. Intell. Transp. Syst.*, vol. 24, no. 4, pp. 4532–4540, Apr. 2023.



Weidong Zhang (Member, IEEE) received the Ph.D. degree in information and communication engineering from the School of Information Science and Technology, Dalian Maritime University, Dalian, China, in June 2022. He is currently a Professor at the School of Information Engineering, Henan Institute of Science and Technology, Xinxiang, China, where he is also the Leader of the Institute of Computer Applications. His current research interests include image restoration, intelligent agriculture, and deep learning. He is also a Senior Member of CCF.



Ling Zhou received the M.S. degree from Huazhong Agricultural University in 2019. She is currently a Teaching Assistant with the Henan Institute of Science and Technology, Xinxiang, China, where she is also with the Institute of Computer Applications. Her research interests include bioinformation technology and intelligent agriculture.



Peixian Zhuang received the Ph.D. degree from the School of Informatics, Xiamen University, Xiamen, China, in 2016. From 2017 to 2020, he was a Lecturer and a Master Supervisor with the School of Electronics and Information Engineering, Nanjing University of Information Science and Technology, Nanjing, China. From 2020 to 2022, he was a Post-Doctoral Fellow and an Assistant Research Fellow with the Department of Automation, Tsinghua University, Beijing, China. He is currently an Associate Professor with the Key Laboratory of Knowledge Automation for Industrial Processes, Ministry of Education, School of Automation and Electrical Engineering, University of Science and Technology Beijing, Beijing. His research interests include sparse representation, Bayesian hierarchical modeling, deep learning, and calcium signal processing.



Wenyi Zhao received the bachelor's degree from the Beijing University of Posts and Telecommunications, Beijing, China, in 2017. He is currently a Post-Doctoral Researcher with the School of Artificial Intelligence, Beijing University of Posts and Telecommunications. His research interests include computer vision, machine learning, deep learning, contrastive learning, and self-supervised learning.



Guohou Li received the Ph.D. degree in control science and engineering from Zhejiang University, Hangzhou, China, in September 2011. He is currently a Professor with the School of Information Engineering, Henan Institute of Science and Technology, Xinxiang, China. His research interests include intelligent control and signal and information processing.



Xipeng Pan received the Ph.D. degree in control science and engineering from the Beijing University of Posts and Telecommunications, China, in 2019. He worked as a Post-Doctoral Researcher with the Department of Radiology, Guangdong Provincial People's Hospital, from August 2020 to November 2022. He is also a Master Supervisor with the School of Computer Science and Information Security, Guilin University of Electronic Technology, China. He has published more than 40 papers. His research interests include machine learning and medical image processing. He is also a member of CCF and ISAIR.



Chongyi Li (Senior Member, IEEE) received the Ph.D. degree from the School of Electrical and Information Engineering, Tianjin University, Tianjin, China, in June 2018. From 2016 to 2017, he was a joint training Ph.D. Student with Australian National University, Australia. He was a Research Fellow with the City University of Hong Kong and Nanyang Technological University from 2018 to 2021. He was a Research Assistance Professor with the School of Computer Science and Engineering, Nanyang Technological University from 2021 to 2023. He is currently a Full Professor at the School of Computer Science, Nankai University, China. His current research focuses on image processing, computer vision, and deep learning, particularly in the domains of image restoration and enhancement.